

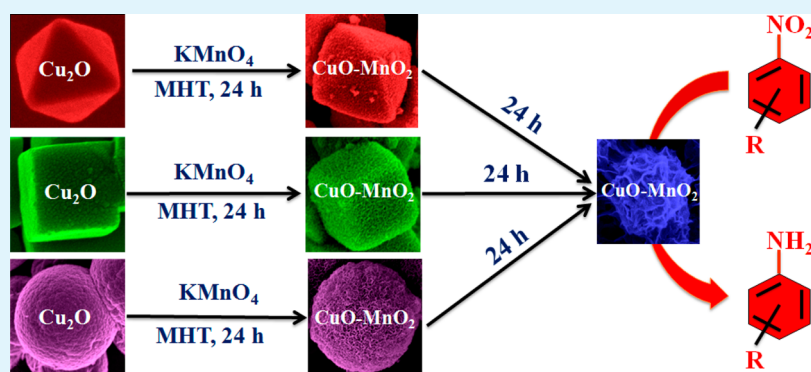
Account of Nitroarene Reduction with Size- and Facet-Controlled CuO–MnO₂ Nanocomposites

Jaya Pal,[†] Chanchal Mondal,[†] Anup Kumar Sasmal,[†] Mainak Ganguly,[†] Yuichi Negishi,[‡] and Tarasankar Pal^{*,†}

[†]Department of Chemistry, Indian Institute of Technology, Kharagpur 721302, India

[‡]Department of Applied Chemistry, Tokyo University of Science, Tokyo 1628601, Japan

S Supporting Information



ABSTRACT: In this work, we propose a systematic and delicate size- and shape-controlled synthesis of CuO–MnO₂ composite nanostructures from time-dependent redox transformation reactions between Cu₂O and KMnO₄. The parental size and shape of Cu₂O nanostructures are retained, even after the redox transformation, but the morphology becomes porous in nature. After prolonged reaction times (>24 h), the product shapes are ruptured, and as a result, tiny spherical porous nanocomposites of ~100 nm in size are obtained. This method is highly advantageous due to its low cost, its easy operation, and a surfactant or stabilizing agent-free approach with high reproducibility, and it provides a facile but new way to fabricate porous CuO–MnO₂ nanocomposites of varied shape and size. The composite nanomaterials act as efficient recyclable catalysts for nitroarene reduction in water at room temperature. The time-dependent reduction kinetics can be easily monitored by using UV–vis spectrophotometer. The catalytic system is found to be very useful toward the reduction of nitro compounds, regardless of the type and position of the substituent(s). Furthermore, it is revealed that CuO–MnO₂ composite nanomaterials exhibit facet-dependent catalytic activity toward nitroarene reduction, where the (111) facet of the composite stands to be more active than that of the (100) facet. The results are also corroborated from the BET surface area measurements. It is worthwhile to mention that porous tiny spheres (product of 48 h reaction) exhibit the highest catalytic activity due to pronounced surface area and smaller size.

KEYWORDS: redox transformation, porous material, facet-dependent, catalysis, CuO–MnO₂

INTRODUCTION

Recently, many efforts have been devoted to the fabrication of nanoparticles due to the fact that the transition from bulk to nanosize regime leads to massive changes in the physical and chemical properties of the nanoparticles.¹ The exponential growth in the field of composite nanomaterials during the past few years is due to their intriguing properties and multiple functionalities. Composite nanomaterials often exhibit superior performances over those of individual nanomaterials in the various fields of application, such as catalysis, biological detection, and optoelectronics.^{2–4} With the passage of time and advancements in the field, the attention is now focused on the synthesis of porous composite materials owing to their huge potential application in adsorption or catalysis.⁵ Porous micro- and nanostructures have come to occupy a distinct position due

to their high surface area, low density, and large pore volumes.⁶ Therefore, exploration of the controllable synthesis of porous micro/nanostructures of composite nanomaterials is now a challenging task.

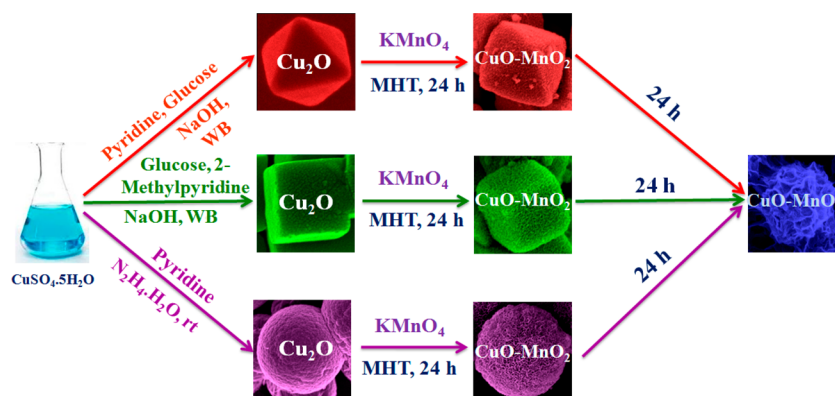
A variety of synthetic protocols in both aqueous and nonaqueous media have been developed for large-scale synthesis of composite nanomaterials.^{7–11} Recently, redox transformation reactions have shown great potential for the synthesis of hollow/porous metal oxide nanoframeworks,^{12,13} alloy nanostructures,¹⁴ and composite nanomaterials.¹¹ Researchers have been paying more attention to exploit the

Received: March 3, 2014

Accepted: May 30, 2014

Published: May 30, 2014

Scheme 1. Schematic Representation of Morphologically Different CuO–MnO₂ Nanocomposites Synthesized from 24 and 48 h Redox Transformation Reactions between Cu₂O (Octahedral, Cubic, and Spherical) Nanoparticles and KMnO₄



technique both in aqueous and organic media to design different nanomaterials with intriguing properties.

As an important p-type transition-metal oxide with a narrow band gap of 1.2 eV, CuO has proved to be a versatile material for applications in catalysis, gas sensors, superconductors, solar cell devices, and lithium ion electrode materials.^{15–19} CuO is an attractive material for its nontoxicity, chemical stability, electrochemical activity, abundant availability, and low production cost.¹¹ On the other hand, MnO₂ is also a promising candidate due to its low cost, high surface area, strong oxidizing/adsorptive ability, and good chemical stability in acidic conditions.²⁰ More significantly, MnO₂ nanoparticles are generally used in pseudocapacitors, heavy metal ion adsorption, catalysis, and gas sensors.^{21–24} By simultaneously taking the advantages of both the nanoparticles, CuO–MnO₂ composite nanomaterial with porous structure has been thought to be an ideal material with great potential to be exploited in catalysis. Only a few studies describe the catalytic activity of CuO–MnO₂ composite nanomaterials. Kun et al. reported that CuO–MnO₂ behaves as an active site for CO oxidation reaction, which follows the interfacial oxidation mechanism.²⁵ Mauricio et al. demonstrated that MnO₂–CuO catalyzes water oxidation for the destruction of quinoline.²⁶ The oxidative conversion of ethyl acetate in water under subcritical and supercritical reaction conditions by using alumina supported MnO₂–CuO catalyst has been reported by Andreas et al.²⁷ So, the progress of catalytic application by using such composite catalyst is highly desirable.

Among the hydrogenation reactions, catalytic hydrogenation of aromatic nitro compounds is now well-received, as the products (aromatic amines) are significant intermediates and precursors in the preparation of pharmaceuticals, polymers, herbicides, agrochemicals, pigments, and dyes.^{28,29} This reaction has been widely used as a model reaction to test the catalytic activity of metal nanoparticles by different groups, including our group,^{30–33} due to two important properties: the reaction does not proceed without a catalyst and the reaction can be easily monitored by UV–vis spectrophotometer. However, the selective reduction of the nitro groups is a challenging task when another reducible group is present in the same molecule. There are many reports on hydrogenation reaction of aromatic nitro compounds by using noble metal catalysts in the presence of NaBH₄.^{34–37} Due to the high cost and limited availability of these types of metals, there is a strong need to develop a suitable catalyst that is more economical, easily available, and nontoxic.

Herein, for the first time, we report the synthesis of size- and shape-dependent CuO–MnO₂ composite nanomaterials from a redox transformation reaction between inexpensive as-synthesized Cu₂O nanoparticles and KMnO₄. Moreover, the morphology can be controlled through the adjustment of reaction time. Meanwhile, all the composite nanomaterials exhibit high surface area due to porous structure and achieve high affinity toward heterogeneous catalysis of nitroarene reduction. In all the cases studied herein, complete conversions of nitroarenes to the corresponding anilines take place within a very short reaction time scale (4–24 min). Our experimental data show that nitroarene reduction depends on many factors such as surface area, porosity, exposed crystal planes, and size.

EXPERIMENTAL SECTION

Materials and Instruments. The related information is presented in the Supporting Information.

Synthesis of Cu₂O Octahedrons, Cubes, and Spheres. In this work, three morphologically different Cu₂O nanoparticles (octahedral, cubic, and spherical) were synthesized according to the previously reported synthetic methods.³⁸ In a typical synthesis, 5 mL of 0.1 M and 10 mL of 0.02 M pyridine solution were added dropwise into the CuSO₄·5H₂O solution (5 mL 0.05 M and 10 mL 0.02 M), and the solution was stirred for 30 min. After the addition of pyridine, blue Cu(OH)₂ colloid was produced within a few minutes. Octahedral Cu₂O nanoparticle (Scheme 1) was obtained when the above reaction mixture was heated in a water bath (WB) for 5 min with 5 mL of 0.1 M glucose solution under alkaline condition (10 mL of 0.1 M NaOH). In contrast, from the well-stirred reaction mixture with hydrazine hydrate (40 μL, 99–100%) at room temperature, we obtained spherical Cu₂O nanoparticle (Scheme 1) in 5 min.

If we use 2-methylpyridine instead of pyridine, then we obtain cubic Cu₂O nanoparticles. Here, 5 mL of 0.1 M 2-methylpyridine solution was added to a CuSO₄·5H₂O solution (5 mL 0.01 M), and the solution was stirred constantly. After the addition of 2-methylpyridine, blue Cu(OH)₂ colloid was formed within a few minutes. Then, 5 mL of 0.1 M glucose solution and 10 mL of 0.1 M NaOH were added to that solution and heated on a water bath for 5 min at ~80 °C. During heating, the solution became red-brown, indicating the formation of Cu₂O nanoparticles with cubic morphology (Scheme 1). Finally, all three types of Cu₂O nanoparticles were carefully washed, first with distilled water and then with absolute ethanol, and dried in vacuum.

Synthesis of CuO–MnO₂ Nanocomposites. For the synthesis of CuO–MnO₂ nanocomposites, 0.01 g of as-synthesized Cu₂O nanoparticles bearing morphologically different shapes was separately dispersed in 5 mL of 0.025 M KMnO₄ solution and stirred vigorously. Then, the three mixtures were taken in screw capped test tubes and heated using a 100 W bulb for different periods of time (24 and 48 h) under modified hydrothermal (MHT) conditions (Scheme 1). The as-

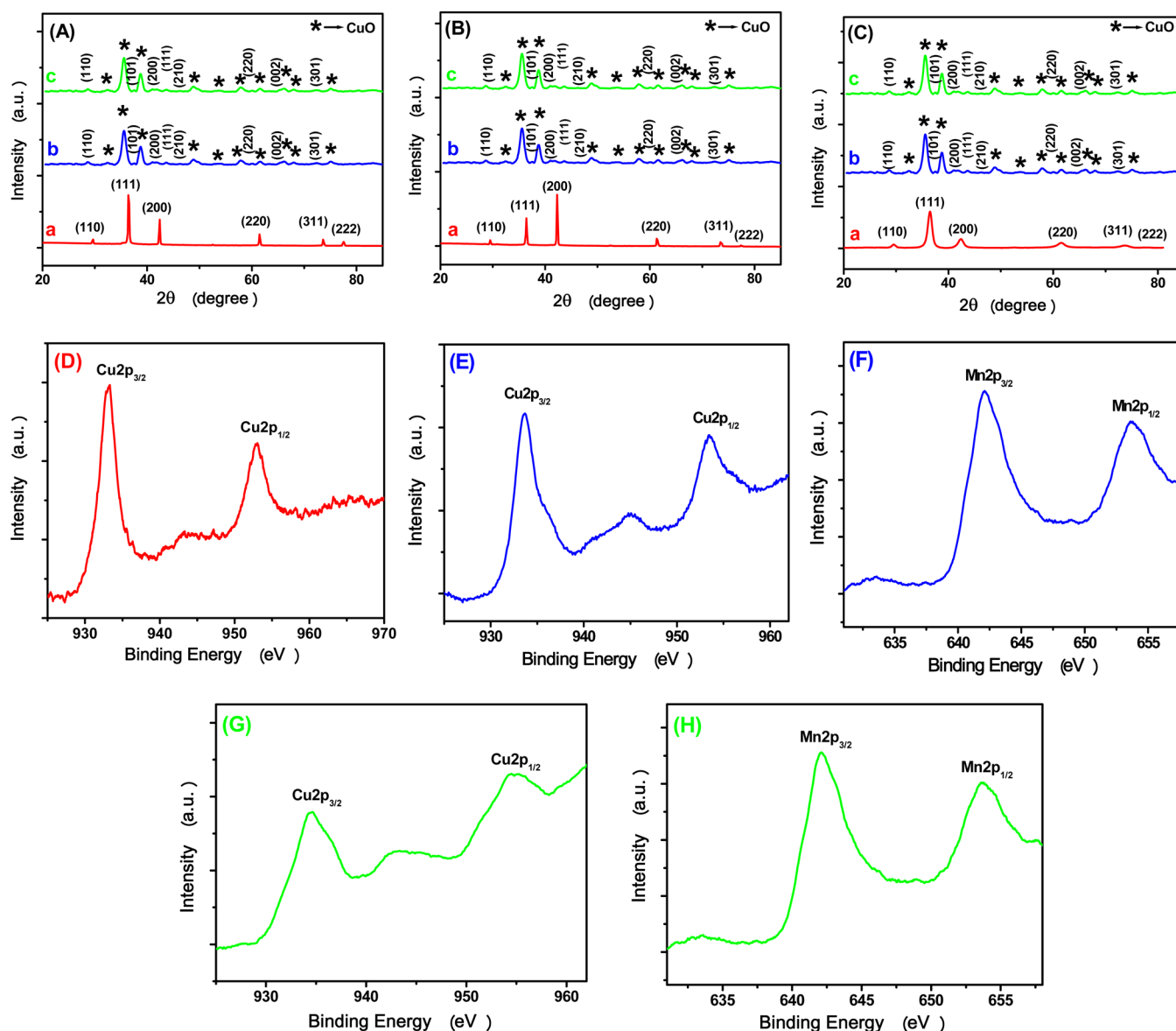


Figure 1. (A–C) Curve a shows the XRD patterns of octahedral, cubic, and spherical Cu_2O nanoparticles, respectively; curves b and c show the XRD patterns of CuO-MnO_2 nanocomposites prepared from 24 and 48 h redox transformation reaction, respectively. (D) Cu 2p XPS spectrum of as-prepared octahedral Cu_2O nanoparticle. XPS spectra of porous octahedral CuO-MnO_2 nanocomposite: (E) Cu 2p spectrum and (F) Mn 2p spectrum. XPS spectra of tiny spherical CuO-MnO_2 nanocomposite: (G) Cu 2p spectrum and (H) Mn 2p spectrum.

obtained black products were carefully washed, first with distilled water and then with absolute ethanol, and dried in vacuum. Finally, all products were annealed at 400°C for 4 h in a controlled air oven, and their unaltered morphologies were examined.

Catalytic Reduction of Nitroarenes. In a typical reaction, 3 mL of 1×10^{-4} M aqueous solution of nitroarene and $300 \mu\text{L}$ of freshly prepared aqueous NaBH_4 (5×10^{-2} M) solution were mixed in a quartz cuvette under ambient conditions. Then, 1 mg of morphologically different CuO-MnO_2 nanocomposites was added to the reaction mixture, and the progress of the reactions was monitored using a UV-vis spectrophotometer. This experiment was also conducted separately with three other catalysts (*viz.*, Cu_2O , CuO , and MnO_2) for comparative study.

RESULTS AND DISCUSSION

X-ray Diffraction Analysis. XRD measurements were performed to determine the phase structures of as-synthesized Cu_2O nanoparticles and CuO-MnO_2 nanocomposites. The a curves in Figure 1A–C display the five reflection peaks at

(110), (111), (200), (220), and (311) for as-prepared octahedral, cubic, and spherical Cu_2O nanoparticles, respectively (JCPDS file No. 05-0667), indicating that all the Cu_2O nanoparticles are phase pure. The (200) diffraction peak in the XRD pattern of cubic Cu_2O nanoparticle is more intense than other diffraction peaks, indicating that cubic Cu_2O exclusively exposes (100) planes, whereas in the case of octahedral Cu_2O , (111) diffraction peak dominates over the other diffraction peaks, indicating that octahedral Cu_2O exclusively exposes (111) planes. The CuO-MnO_2 composite nanoparticle (before annealing at 400°C for 4 h) does not exhibit any signature of MnO_2 (Figure S1a of the Supporting Information). However, EDX analysis (Figure S1b of the Supporting Information) reveals the presence of Mn in the composite. This is presumably due to the amorphous nature of MnO_2 . To confirm the presence of MnO_2 , we annealed the sample at 400°C for 4 h and observed the expected crystalline MnO_2 in the

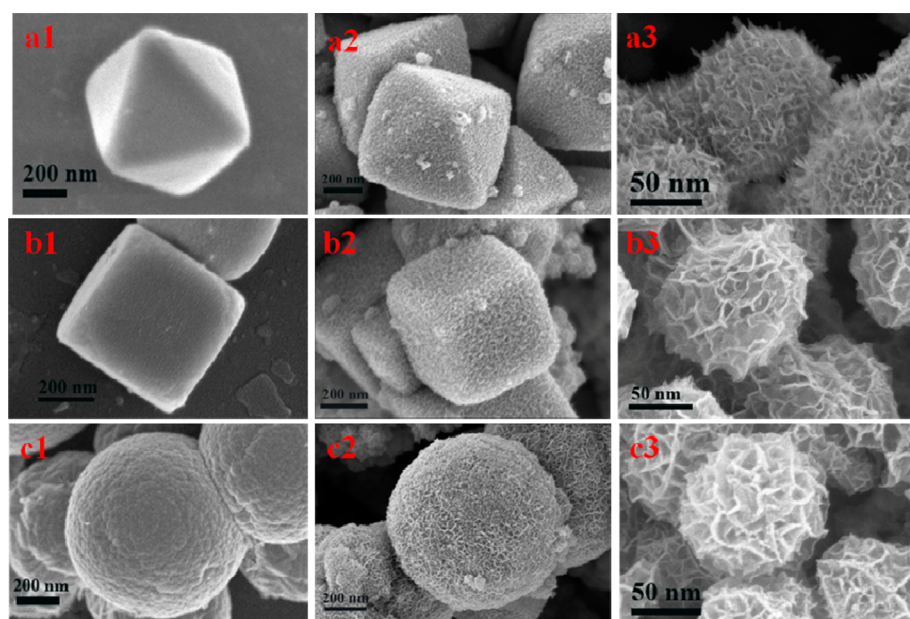


Figure 2. FESEM images of as-synthesized (a1) octahedral, (b1) cubic, and (c1) spherical Cu_2O nanoparticles. (a2, b2, and c2) and (a3, b3, and c3) FESEM images of CuO-MnO_2 nanocomposites prepared from 24 and 48 h redox transformation reactions between (a1) octahedral, (b1) cubic, and (c1) spherical Cu_2O nanoparticles and KMnO_4 , respectively.

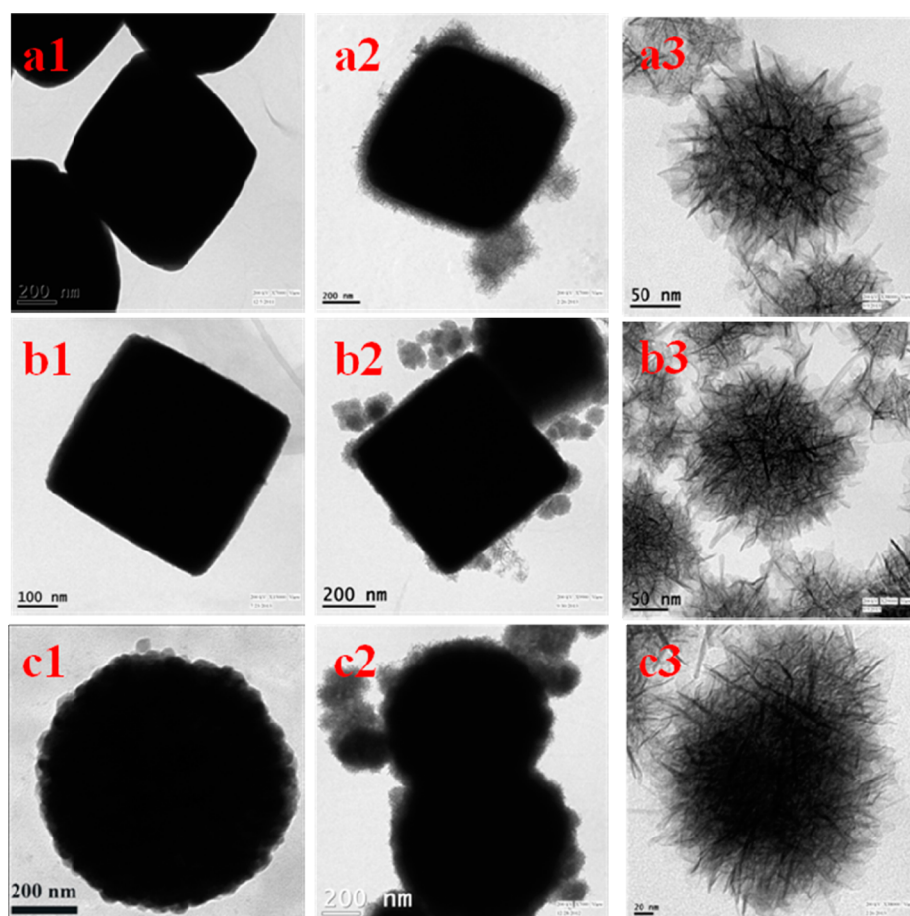


Figure 3. TEM images of as-synthesized (a1) octahedral, (b1) cubic, and (c1) spherical Cu_2O nanoparticles. (a2, b2, and c2) and (a3, b3, and c3) TEM images of CuO-MnO_2 nanocomposites prepared from 24 and 48 h redox transformation reactions between (a1) octahedral, (b1) cubic, and (c1) spherical Cu_2O nanoparticles and KMnO_4 , respectively.

sample by XRD measurement. So, the presence of amorphous MnO_2 was explicitly assured. The b and c curves in Figure 1A–

C represent the XRD patterns of CuO-MnO_2 nanocomposites prepared from 24 and 48 h redox transformation reaction

between Cu₂O (octahedral, cubic, and spherical) and KMnO₄ followed by annealing at 400 °C for 4 h. Here, all the diffraction peaks in the XRD patterns of CuO–MnO₂ nanocomposites obtained at different time intervals (24 and 48 h) are the same. The diffraction peaks at $2\theta = 32.4^\circ, 35.6^\circ, 38.8^\circ, 48.8^\circ, 53.6^\circ, 58.1^\circ, 61.5^\circ, 66.1^\circ, 68.1^\circ,$ and 74.9° correspond to (110), (1 $\bar{1}$ 1) and (002), (111) and (200), (2 $\bar{0}$ 2), (020), (202), (1 $\bar{1}$ 3), (1 $\bar{1}$ 3), (220), and (004) planes for CuO nanoparticle (JCPDS file No. 48-1548) and the other peaks at $2\theta = 28.7^\circ, 37.4^\circ, 41.1^\circ, 43.4^\circ, 46.3^\circ, 59.9^\circ, 65.3^\circ,$ and 72.4° correspond to (110), (101), (200), (111), (210), (220), (002), and (301) for β -MnO₂ (JCPDS file No. 72-1984). These experimental results imply that Cu₂O nanoparticles are completely converted to CuO–MnO₂ composite nanomaterials.

XPS Analysis. With the help of XPS analysis, the chemical state and surface atomic composition of both Cu₂O nanoparticles and CuO–MnO₂ composite nanomaterials have been authenticated. Figure S2a of the Supporting Information exhibits main core level peaks for C 1s, O 1s, and Cu 2p at binding energies of 284.6, 530.3, and 932.5 eV, respectively. The high-resolution XPS spectrum shows the peaks of Cu 2p_{3/2} and Cu 2p_{1/2} at 932.5 and 952.8 eV, respectively, arising from octahedral Cu₂O nanoparticle (Figure 1D).¹¹ A few shakeup satellite peaks are also noticed at the higher energy side in the spectrum, 940.4 and 943.1 eV, which can be attributed to Cu(II) states.¹¹ These facts propose the existence of a thin layer of CuO on the Cu₂O surface due to surface oxidation. The survey scan spectrum of CuO–MnO₂ nanocomposite obtained from 24 h redox transformation reaction between octahedral Cu₂O and KMnO₄ shows the presence of C 1s, O 1s, Cu 2p and Mn 2p peaks (Figure S2b of the Supporting Information). The XPS spectra of Cu 2p_{3/2} and Cu 2p_{1/2} at 933.5 and 953.5 eV are attributed to the presence of CuO (Figure 1E).¹¹ The high-resolution XPS spectrum (Figure 1F) displays two peaks at 642.1 and 653.7 eV, which are the characteristic Mn 2p_{3/2} and Mn 2p_{1/2} peaks of β -MnO₂.³⁹ Figure 1G,H and Figure S2c of the Supporting Information show the XPS spectra of CuO–MnO₂ composite nanomaterial synthesized from 48 h redox transformation reaction between octahedral Cu₂O and KMnO₄. Here, the main core level peak positions for C 1s, O 1s, Cu 2p, and Mn 2p are similar to those of the above CuO–MnO₂ nanocomposite. So, the composition and chemical nature of both the composite nanomaterials prepared from different time intervals are the same. Similar results are also observed from the XPS spectra of cubic and spherical Cu₂O nanoparticles before and after the redox transformation reaction with KMnO₄ at different time intervals.

FESEM and TEM Analysis. To determine the 3D architecture of the as-synthesized Cu₂O nanoparticles as well as CuO–MnO₂ composite nanomaterials, FESEM and TEM measurements were performed. FESEM (a1 in Figure 2 and Figure S3 of the Supporting Information) and TEM images (a1 in Figure 3 and Figure S4 of the Supporting Information) show the well-defined, smooth, and uniform morphology of octahedral Cu₂O nanoparticles with octahedral edge length of 600–630 nm. FESEM (a2 in Figure 2 and Figure S3 of the Supporting Information) and TEM images (a2 in Figure 3 and Figure S4 of the Supporting Information) reveal the porous octahedral morphology of CuO–MnO₂ composite nanomaterial obtained after 24 h of redox transformation reaction. In this case, octahedral edge length remains same as that of octahedral Cu₂O. When the redox transformation reaction was continued for 48 h, the tiny spherical CuO–MnO₂ was

obtained with an extremely porous structure. The average diameter of the tiny spherical CuO–MnO₂ is about 100 nm. This result is confirmed by FESEM (a3 in Figure 2 and Figure S3 of the Supporting Information) and TEM images (a3 in Figure 3 and Figure S4 of the Supporting Information).

FESEM (b1 in Figure 2 and Figure S3 of the Supporting Information) and TEM images (b1 in Figure 3 and Figure S4 of the Supporting Information) exhibit well-defined, smooth, and uniform morphology of the cubic Cu₂O nanoparticles with average edge length of 400–430 nm. When the redox reaction was allowed to progress for 24 h, the porous structure of cubic CuO–MnO₂ with average edge length of 400–430 nm was observed from FESEM (b2 in Figure 2 and Figure S3 of the Supporting Information) and TEM images (b2 in Figure 3 and Figure S4 of the Supporting Information). FESEM (b3 in Figure 2 and Figure S3 of the Supporting Information) and TEM images (b3 in Figure 3 and Figure S4 of the Supporting Information) show tiny spherical CuO–MnO₂ with highly porous nature (average diameter 100 nm) when the redox reaction time is increased to 48 h.

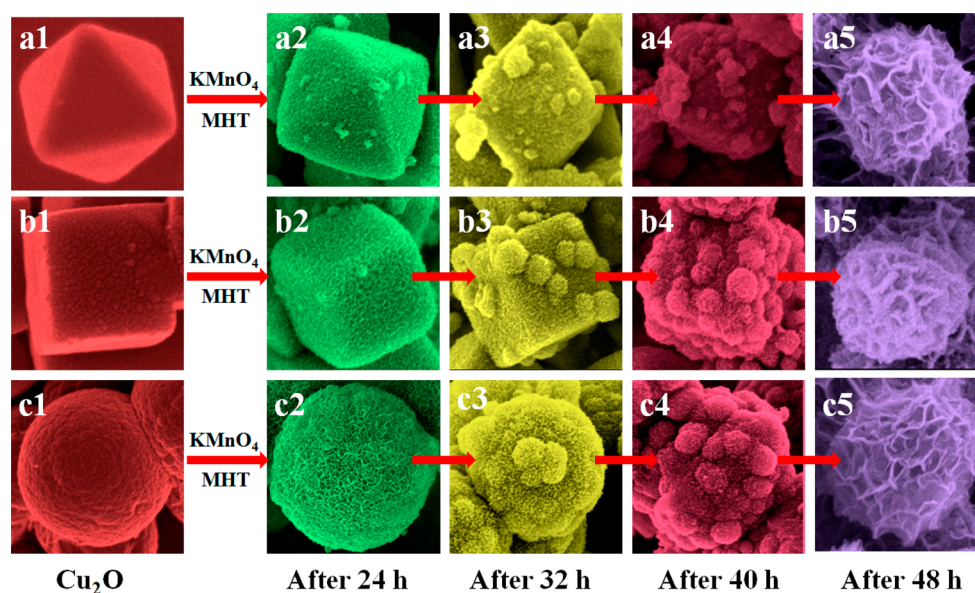
FESEM (c1 in Figure 2 and Figure S3 of the Supporting Information) and TEM images (c1 in Figure 3 and Figure S4 of the Supporting Information) display well-defined and uniform morphology of spherical Cu₂O nanoparticles with an average diameter of 800 nm. FESEM (c2 in Figure 2 and Figure S3 of the Supporting Information) and TEM images (c2 in Figure 3 and Figure S4 of the Supporting Information) indicate that the surface of spherical CuO–MnO₂ (average diameter of 800 nm) is porous when the redox reaction time is 24 h. The 48 h redox transformation reaction causes the formation of highly porous CuO–MnO₂ with tiny spherical structure (average diameter of 100 nm), as shown in FESEM (c3 in Figure 2 and Figure S3 of the Supporting Information) and TEM images (c3 in Figure 3 and Figure S4 of the Supporting Information). In all three cases, it is observed that structure and morphology of CuO–MnO₂ composite nanomaterials (average diameter of 100 nm) obtained from the 48 h redox transformation reaction between Cu₂O (octahedral, cubic, and spherical) and KMnO₄ are alike. XRD results (curve c in Figure 1A–C) also reveal that the composition of these final products obtained from three different reaction mixtures is also the same.

BET Measurements of CuO–MnO₂ Composite Nanomaterials. Surface area of the composite nanomaterials plays a crucial role for catalytic application. To augment the proposition, the surface area of differently shaped CuO–MnO₂ nanocomposites was measured from BET experiment (Figure S5 of the Supporting Information). The surface area of the tiny spherical, octahedral, cubic, and spherical CuO–MnO₂ composite nanomaterials was found to be 88.321, 51.925, 47.576, and 36.289 m²/g, respectively (Table 1). The pore volumes of the nanomaterials are 3.182×10^{-01} , 1.96×10^{-01} , 1.65×10^{-01} , 6.88×10^{-02} cm³/g, respectively (Table 1). The

Table 1. BET Surface Area, Pore Volume, and Rate Constant for Different CuO–MnO₂ Composite Nanomaterials

composite nanomaterial	surface area (m ² /g)	pore volume (cm ³ /g)	rate constant (min ⁻¹)
tiny spherical CuO–MnO ₂	88.321	3.182×10^{-01}	0.3136
octahedral CuO–MnO ₂	51.925	1.96×10^{-01}	0.2625
cubic CuO–MnO ₂	47.576	1.65×10^{-01}	0.1904
spherical CuO–MnO ₂	36.289	6.88×10^{-02}	0.1724

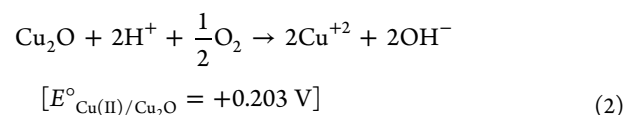
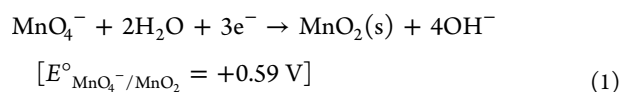
Scheme 2. Schematic Representation of Time-Dependent Growth Process To Obtain Tiny Spherical CuO–MnO₂ Nanocomposites from As-Synthesized Cu₂O Nanoparticles^a



^aComposites a2, b2, and c2 obtained after 24 h of reaction; a3, b3, and c3 obtained after 32 h of reaction; a4, b4, and c4 obtained after 40 h of reaction; and a5, b5, and c5 obtained after 48 h of reaction from (a1) octahedral, (b1) cubic, and (c1) spherical Cu₂O nanoparticles, respectively.

results support the surface-area-related catalytic activity toward the proposed nitroarene reduction.

Formation Mechanism of Morphologically Different Shaped CuO–MnO₂ Composite Nanomaterials. Here, a simple, facile, cost-effective and surfactant-free synthetic strategy has been described for the evolution of CuO–MnO₂ composite nanomaterials. The porous CuO–MnO₂ nanocomposites are prepared in a two-step process. According to the preparation strategy, the first step involves the formation of octahedral, cubic, and spherical Cu₂O nanoparticles by using different hydrolyzing and reducing agents. The formation mechanism of differently shaped Cu₂O nanoparticles has already been discussed in our previous work.³⁸ The second step is the synthesis of CuO–MnO₂ nanocomposites by employing a redox transformation reaction between Cu₂O (octahedral, cubic, and spherical) nanoparticles and KMnO₄ solution under MHT condition for 24 and 48 h. The standard reduction potential values of MnO₄[−]/MnO₂ (+ 0.59 V vs SHE) and Cu²⁺/Cu₂O (+ 0.203 V vs SHE) pairs prescribe thermodynamically allowed formation of CuO–MnO₂ nanocomposite. Controlled temperature and autogenic pressure of the modified hydrothermal (MHT) conditions and final pH (~7.5) of the reaction mixture play significant roles in the formation of composite nanomaterials. When the redox transformation reaction is initiated, Cu₂O is oxidized to Cu²⁺ (tested with potassium ferrocyanide) with continuous stripping of electrons from the surface, which are transferred to the MnO₄[−] ions, causing the formation of MnO₂ nanoparticles. The formation of CuO takes place most probably through the dehydration of Cu(OH)₂ under MHT condition.



We have studied the shape and morphology evolution of the composite nanomaterials in different time domains to explain the growth mechanism of the final products, and the results are presented in Scheme 2 (FESEM images). After the samples incubated for 24 h, we notice the formation of porous octahedral, cubic, and spherical CuO–MnO₂ nanocomposite with the retention of parental size and shape of Cu₂O nanostructures. When the incubation time is increased to 32 h, nanospherical overgrowth is observed all over the surface of octahedral, cubic, and spherical CuO–MnO₂. Densely packed overgrowth of nanospherical particles throughout the surfaces is created when the incubation time is increased to 40 h. When the incubation time is prolonged further to 48 h, octahedral, cubic, and spherical CuO–MnO₂ nanoparticles with complete coverage of spherical superstructures are found to be ruptured into tiny spherical nanocomposites with an average diameter of 100 nm.

After comparing the sizes of the respective metal ions involved in the redox transformation process, it may be concluded that the smallest Mn^{IV} (67 pm) is incorporated conveniently in the crystal lattice of the larger Cu^{II} (87 pm) assembly originated from Cu^I (91 pm). An almost 20% density reduction of the composite (revealed from specific gravity measurement) speaks in favor of porous structure. Thus, the comparative size factor of the metal ions accounts the Mn^{IV} incorporation into the CuO matrix, and low-density porous composite formation results.

Catalysis. Morphology-dependent^{40–43} and facet-selective^{44–49} catalytic activity has now become an effective and popular way to study chemical transformation. To explore the ability and performance of the as-synthesized CuO–MnO₂

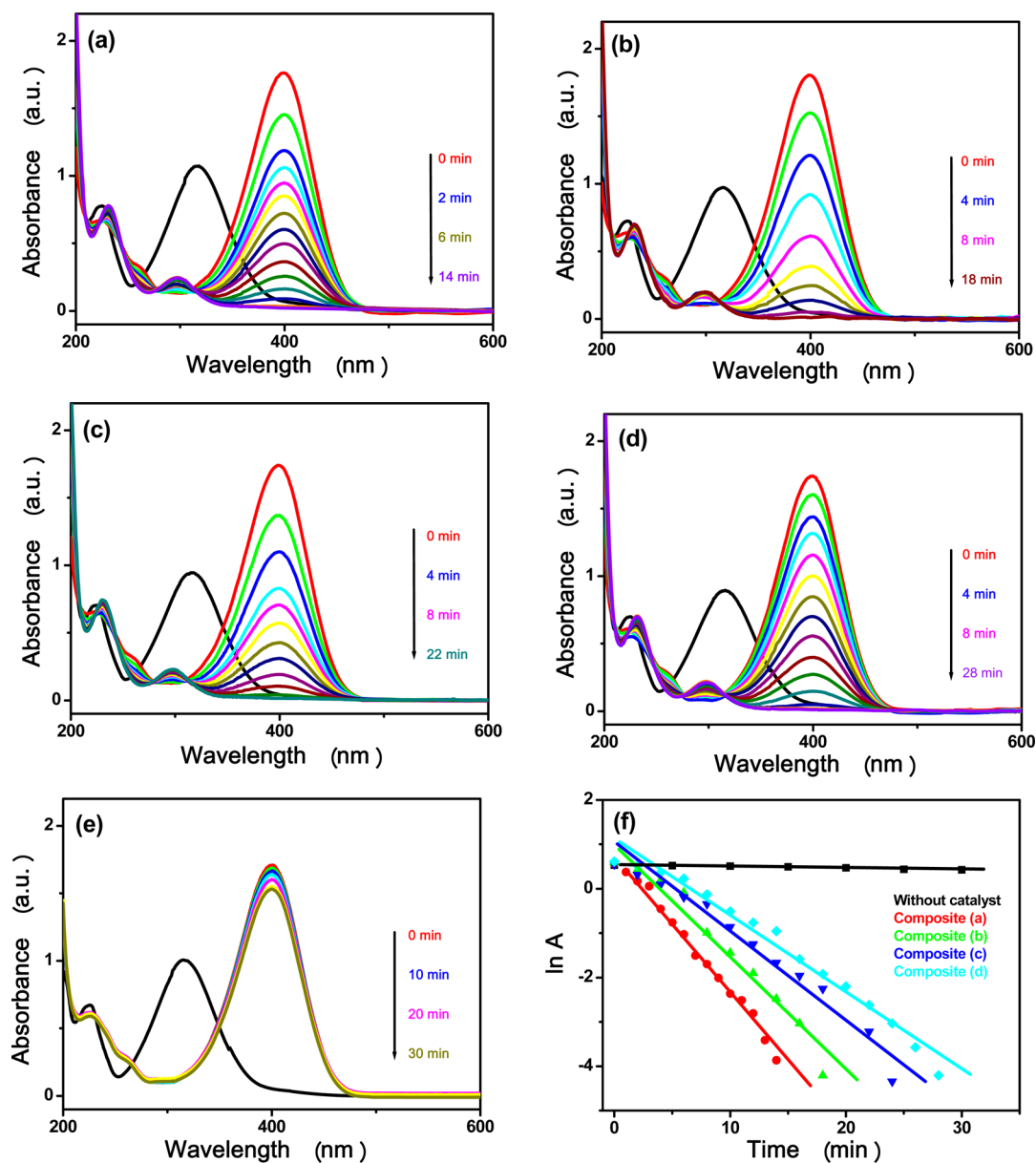


Figure 4. UV-visible absorption spectra of the reduction of 4-nitrophenol by NaBH_4 in the presence of 1 mg of (a) tiny spherical, (b) octahedral, (c) cubic, and (d) spherical CuO-MnO_2 catalyst and (e) without catalyst. (f) Corresponding $\ln A$ vs time plot.

nanocomposites as a catalyst, we have performed hydrogenation reaction of various nitrocompounds in the presence of NaBH_4 as a hydrogen source. Because nitroarenes are a class of toxic and poisonous chemicals, a number of catalytic methods for the reduction of nitroarenes have been developed to accomplish this transformation.⁵⁰ In the absence of any catalyst, the reaction does not proceed favorably (Figure 4e).

To investigate the catalytic efficiency of differently shaped CuO-MnO_2 composite nanomaterials, we first studied the reduction of 4-nitrophenol in the presence of NaBH_4 . It is well-known that aqueous 4-nitrophenol solution shows a strong absorption peak at 317 nm, but in the presence of NaBH_4 solution, the peak is remarkably red-shifted to 400 nm. This is mainly due to the formation of dark yellow colored nitrophenolate ions in alkaline condition. During the reduction process (in the presence of a catalyst), the characteristic band of 4-nitrophenolate ions at 400 nm is gradually diminished with time, and a new concomitant peak arises at 300 nm due to the

formation of colorless 4-aminophenol. Time-dependent reduction kinetics of this reduction reaction can be easily monitored by using a UV-vis spectrophotometer. In our study, 1 mg of the CuO-MnO_2 nanocomposite was added to 3 mL of a 1×10^{-4} M aqueous solution of 4-nitrophenol in the presence of a freshly prepared aqueous NaBH_4 (300 μL ; 5×10^{-2} M) solution in ambient conditions. In the absorbance spectra, two isosbestic points are created at around 280 and 313 nm, which suggests 4-aminophenol as a sole product with no other byproducts.³³ Because the added NaBH_4 has much higher concentration (500 times) relative to the 4-NP, the catalytic reaction follows pseudo-first-order reaction kinetics, and the plot of $\ln A$ vs time demonstrates a straight line with a negative slope to point out the rate constant. Figure 4a–d shows UV-vis absorption spectra of the 4-NP reduction for tiny spherical, octahedral, cubic, and spherical CuO-MnO_2 nanocomposites, respectively. Catalytic efficiency toward 4-NP reduction by morphologically different shapes of CuO-MnO_2 nanocompo-

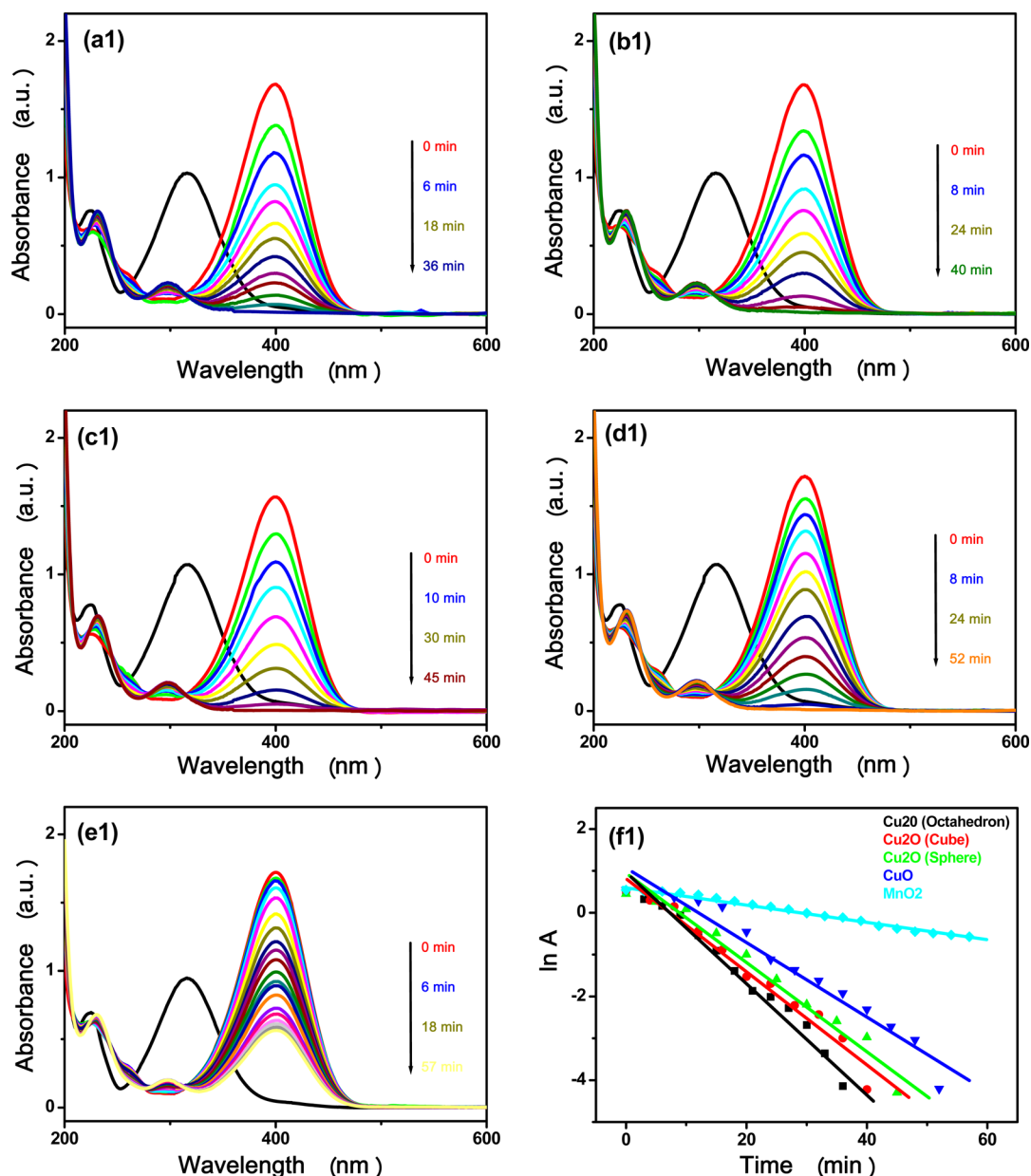


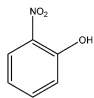
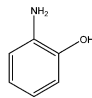
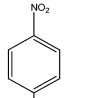
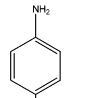
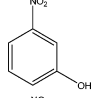
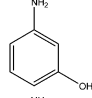
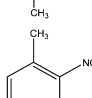
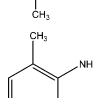
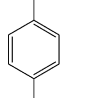
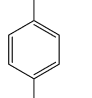
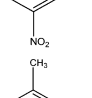
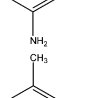
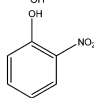
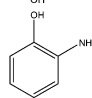
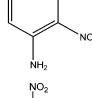
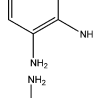
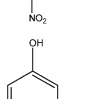
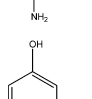
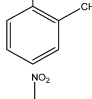
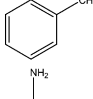
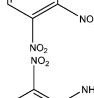
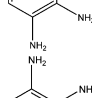
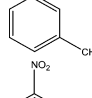
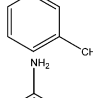
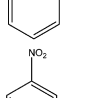
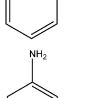
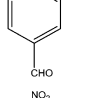
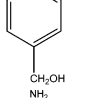
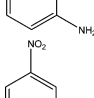
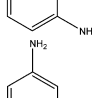
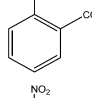
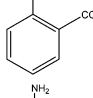
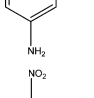
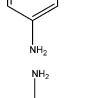
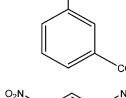
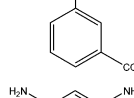
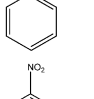
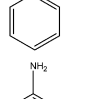
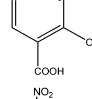
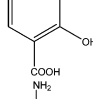
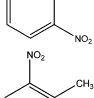
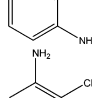
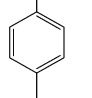
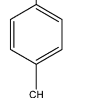
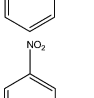
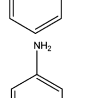
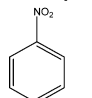
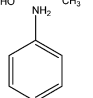
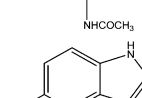
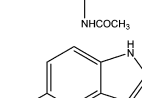
Figure 5. UV–visible absorption spectra of the reduction of 4-nitrophenol by NaBH_4 in the presence of 1 mg of (a1) octahedral, (b1) cubic, and (c1) spherical Cu_2O catalyst; (d1) CuO ; and (e1) MnO_2 catalyst. (f1) Corresponding $\ln A$ vs time plot.

sites follows the sequence of (a) tiny sphere > (b) octahedron > (c) cube > (d) sphere (Table S1 of the Supporting Information). On the basis of the results of FESEM and TEM, it can be concluded that all the CuO-MnO_2 nanocomposites exhibit a porous structure with a large void space within it. From BET measurement, the surface areas of the differently shaped CuO-MnO_2 nanocomposites follow the order of (a) tiny sphere > (b) octahedron > (c) cube > (d) sphere. Considering the BET results, we concluded that the catalytic efficiency of these composite nanomaterials has a close relationship with the surface area, as generally expected. Octahedral CuO-MnO_2 is bound by eight triangular (111) facets, whereas cubic CuO-MnO_2 is composed of six (100) facets. It is known that (100) facets are less reactive than (111) facets.^{38,51} So, the octahedral CuO-MnO_2 exhibits greater catalytic efficiency than that of the cubic CuO-MnO_2 nanocomposites. This is also supported from BET results.

The lowest catalytic efficiency of spherical particles (800 nm) is ascribed to its lowest surface area. It has been found that the tiny spherical CuO-MnO_2 with average diameter of 100 nm can be successfully fabricated only by increasing the redox reaction time to 48 h, and these tiny spherical nanocomposites exhibit the highest catalytic efficiency. So, the small particle size, porous structure, and high surface area of the tiny spherical CuO-MnO_2 make them most promising catalyst for 4-NP reduction than the other three composite nanoparticles. The plots of $\ln A$ vs time (min) for different CuO-MnO_2 catalysts show straight lines with negative slopes (Figure 4f). The values of rate constant for tiny spherical, octahedral, cubic, and spherical CuO-MnO_2 nanocomposites (1 mg) are 0.3136, 0.2625, 0.1904, and 0.1724 min^{-1} , respectively.

To demonstrate a comparative account of catalytic efficiency, we have performed the same experiments individually by using the as-synthesized Cu_2O (octahedral, cubic, and spherical),

Table 2. Reduction of Various Nitroarenes Using Tiny Spherical CuO–MnO₂ Nanocatalyst

Entry	Substrate	Product	Time (min)	Entry	Substrate	Product	Time (min)
1			11	13			18
2			7	14			14
3			14	15			10
4			9	16			6
5			15	17			14
6			15	18			10.5
7			10	19			5
8			21	20			14
9			22	21			9
10			8	22			4
11			24	23			6
12			22	24			7
							

CuO (synthesized following a reported method⁵²), and MnO₂ (synthesized following a reported method³⁹) nanoparticles as catalyst. Figure 5a1–c1 displays UV–vis absorption spectra of the 4-NP reduction for octahedral, cubic, and spherical Cu₂O nanoparticles, respectively, keeping all other reaction conditions unaltered. The order of catalytic reactivity of differently shaped Cu₂O nanoparticles is as follows: (a1) octahedron > (b1) cube > (c1) sphere (Table S1 of the Supporting Information), and the reason is similar to that of CuO–MnO₂ nanocomposites. As can be seen from Figure 5d1,e1, CuO nanoparticle takes

shorter time than MnO₂ nanoparticles and longer time than Cu₂O to complete the reduction of 4-NP under the same prescribed experimental conditions. The plots ln A vs time (min) for different Cu₂O (octahedral, cubic, and spherical), CuO, and MnO₂ nanoparticles exhibit straight lines with negative slopes (Figure 5f1). The values of rate constant for octahedral Cu₂O, cubic Cu₂O, spherical Cu₂O, CuO, and MnO₂ nanoparticles (1 mg) are 0.1251, 0.1112, 0.1023, 0.0876, and 0.0217 min⁻¹, respectively. It is worth mentioning that the reaction does not proceed in the absence of catalyst (Figure

4e). In this comparative study, we observed that our composite nanomaterials serve as better catalyst than the individual and neat Cu_2O , CuO , and MnO_2 nanoparticles, and the final order of the catalytic efficiency is as follows: tiny spherical CuO-MnO_2 > octahedral CuO-MnO_2 > cubic CuO-MnO_2 > spherical CuO-MnO_2 > octahedral Cu_2O > cubic Cu_2O > spherical Cu_2O > CuO > MnO_2 (Table S1 of the Supporting Information). From this comparative analysis, it is clearly found that only 65% reduction of nitroarene takes place with MnO_2 nanomaterial (Figure S1), on the basis of which we consider MnO_2 almost as an inert component of the composite material.^{53,54} Here, KMnO_4 oxidizes Cu_2O to facet-exposed CuO with increasing surface area. Eventually, porosity is inherited by the composites, and at the same time, KMnO_4 reduces to MnO_2 . This study clearly points out that the presence of a porous composite nanomaterial is most complementary to make 4-NP reduction facile. The best catalytic performance comes from the smallest spherical particles with the highest surface area of the tiny spheres, the sole product of the 48 h KMnO_4 mediated redox reaction. But recall that the facet-selective catalytic rate comparison excludes tiny spheres.

To ensure the catalytic activity of the tiny composite toward the reduction of nitro group in general, we have examined a series of nitroarenes with structurally divergent groups, keeping all other reaction conditions unaltered (Figures S6 and S7 of the Supporting Information). As shown in Table 2, the catalyst CuO-MnO_2 (tiny sphere) was found to be very active toward the reduction of nitro compounds, regardless of the types and position of the substituent(s). Here, we observed that reduction of unsubstituted nitrobenzene required much longer reaction time (22 min) than the substituted nitrobenzene. Explicitly 2-, 3-, and 4-nitrophenols in a shorter time span (7–14 min) produce corresponding anilines (Figure S6, panels 1–3, of the Supporting Information and Table 2), and 3-nitrophenol shows the highest reactivity among all the three nitrophenols. It is a well-established fact that the reaction proceeds through the formation of a nitrophenolate ion, and 4-nitrophenolate ion is most stable because of resonance stabilization, whereas 2-nitrophenolate ion is somewhat less stable than 4-nitrophenolate ion due to some degree of steric effect. Due to the lack of resonance stabilization, 3-nitrophenol becomes least stable and hence most reactive than the other two isomers.³¹ A similar explanation holds for nitroanilines, and 3-nitroaniline is found to be the most reactive among all the three nitroanilines (Figure S6, panels 6–8, of the Supporting Information and Table 2). Reduction of nitrotoluene generally takes a somewhat longer time to produce the corresponding aniline than other nitroarenes mainly due to the presence of an electron-donating group such as $-\text{CH}_3$ (Table 2). The reduction reaction of the nitro group in the presence of other functionalities such as $-\text{CHO}$, $-\text{COMe}$, $-\text{NHCOMe}$, and $-\text{COOH}$ has also been performed. In the case of 2-, 3-, and 4-nitrobenzaldehyde and 4-nitroacetophenone, $-\text{CHO}$ and $-\text{COMe}$ groups are also reduced along with the reduction of the nitro group (confirmed by ^1H NMR; Figures S8–S11 of the Supporting Information). Under the same reaction conditions, the $-\text{NHCOMe}$ and $-\text{COOH}$ groups remain totally unchanged.

The reduction of nitroarenes takes place presumably on the catalyst surface. NaBH_4 is the reductant, and it is pertinent to consider the reduction of CuO to $\text{Cu}(0)$. As a result of this thermodynamically favorable reduction, the reduction reaction possibly takes place on the Cu surface, and MnO_2 extends its

support as an inert material. $\text{Cu}(0)$ surface then houses the BH_4^- ion along with the respective nitroarene.³⁰ Here, the electron transfer takes place, and nitroarene is reduced. However, at the end of the reduction, the $\text{Cu}(0)$ surface is oxidized to CuO in aqueous alkaline conditions ($\text{pH} \sim 14$).⁵⁵ Thus, we get back the composite catalyst material, which is authenticated from the XRD analysis (Figure S12c of the Supporting Information) of the recycled catalyst.

After the hydrogenation reaction was complete, the catalysts were separated from the reaction mixture by centrifugation and washed thoroughly with distilled water and ethanol. The dried catalysts were examined by XRD (Figure S12c of the Supporting Information), and morphologies were ascertained again by FESEM (Figure S12a and S12b of the Supporting Information) and TEM analysis (Figure S12d of the Supporting Information). The above analysis demonstrates that the composition and morphology of the catalysts remain unaltered. The catalyst is found to be recyclable, even after four consecutive cycles.

CONCLUSIONS

In summary, we demonstrate a simple, facile, and surfactant-free redox transformation approach to fabricate crystallographic surfaces of different CuO-MnO_2 composite nanomaterials with the retention of parental size and shape of Cu_2O , the notable starting material. Morphologically different CuO-MnO_2 nanocomposites are found to be ruptured into tiny spherical nanocomposites with the increase of reaction time. The synthetic process represents a new way to systematically direct the size- and shape-controlled synthesis of porous composite nanomaterials. All the composite nanomaterials could achieve high efficiency toward nitroarene reduction due to its porous nature. No additives or promoters are required for the reaction. In addition, we have also demonstrated that the as-prepared composite nanomaterials show size- and facet-dependent catalytic activity. We reveal that the catalytic activity of CuO-MnO_2 exposing (111) planes performs better than that of (100) plane. The catalytic efficiency of the CuO-MnO_2 composite nanomaterials has been found to be related to the experimentally determined surface area of the materials. Furthermore, the large surface area, porous structure, and small particle size of tiny spherical CuO-MnO_2 make it a promising material for shouldering the highest catalytic activity. The reduction of the nitro functionality, as usual, has been observed to be independent of the substituent(s). The easy operation for the deliverable catalyst, a short reaction time, mild reaction conditions, and aqueous medium at room temperature make the catalytic system economical, green, and environmentally friendly for the reduction of nitroarenes.

ASSOCIATED CONTENT

Supporting Information

Details about chemicals, analytical instruments, SAED patterns, HRTEM, area mapping analysis, composition determination, and spectroscopic data of the products; XRD and EDX analysis of the composite before annealing; wide-range XPS spectra, FESEM, TEM images, nitrogen adsorption–desorption isotherm, ^1H NMR spectra, SAED patterns, HRTEM image, EDX, and area mapping analysis; UV–vis absorption spectra of different nitroarenes; FESEM, TEM, and XRD analysis of the catalyst after reaction; and a comparative account of different catalysts for 4-NP reduction. This material is available free of charge via the Internet at <http://pubs.acs.org>.

AUTHOR INFORMATION

Corresponding Author

*E-mail: tpal@chem.iitkgp.ernet.in.

Notes

The authors declare no competing financial interest.

ACKNOWLEDGMENTS

The authors are thankful to the UGC, DST, BRNS, and CSIR New Delhi for financial assistance and IIT Kharagpur for research facilities. The authors are also thankful to Miss Isozaki of Tokyo University of Science, Tokyo, Japan, for XPS measurements.

REFERENCES

- (1) Astruc, D.; *Nanoparticles and Catalysis*; Wiley-VCH: New York, 2008.
- (2) Kazes, M.; Lewis, D. Y.; Banin, U. Method for Preparation of Semiconductor Quantum-Rod Lasers in a Cylindrical Microcavity. *Adv. Funct. Mater.* **2004**, *14*, 957–962.
- (3) Xu, C.; Xie, J.; Ho, D.; Wang, C.; Kohler, N.; Walsh, E. G.; Morgan, J. R.; Chin, Y. E.; Sun, S. Au-Fe₃O₄ Dumbbell Nanoparticles as Dual-Functional Probes. *Angew. Chem., Int. Ed.* **2008**, *47*, 173–176.
- (4) Choi, J.-S.; Jun, Y.-W.; Yeon, S.-I.; Kim, H. C.; Shin, J.-S.; Cheon, J. Biocompatible Heterostructured Nanoparticles for Multimodal Biological Detection. *J. Am. Chem. Soc.* **2006**, *128*, 15982–15983.
- (5) Bao, L.; Zang, J.; Li, X. Flexible Zn₂SnO₄/MnO₂ Core/Shell Nanocable–Carbon Microfiber Hybrid Composites for High-Performance Supercapacitor Electrodes. *Nano Lett.* **2011**, *11*, 1215–1220.
- (6) Kresge, C. T.; Leonowicz, M. E.; Roth, W. J.; Vartuli, J. C.; Beck, J. S. Ordered Mesoporous Molecular Sieves Synthesized by a Liquid-Crystal Template Mechanism. *Nature* **1992**, *359*, 710–712.
- (7) Zhang, M.; Lei, D.; Yin, X.; Chen, L.; Li, Q.; Wang, Y.; Wang, T. Magnetite/Graphene Composites: Microwave Irradiation Synthesis and Enhanced Cycling and Rate Performances for Lithium Ion Batteries. *J. Mater. Chem.* **2010**, *20*, 5538–5543.
- (8) Li, Z.; Hou, B.; Xu, Y.; Wu, D.; Sun, Y.; Hu, W.; Deng, F. Comparative Study of Sol–Gel-Hydrothermal and Sol–Gel Synthesis of Titania–Silica Composite Nanoparticles. *J. Solid State Chem.* **2005**, *178*, 1395–1405.
- (9) Yang, H.; Song, X.; Zhang, X.; Ao, W.; Qiu, G. Synthesis of Vanadium-Doped SnO₂ Nanoparticles by Chemical Co-Precipitation Method. *Mater. Lett.* **2003**, *57*, 3124–3127.
- (10) Jiang, H.; Dai, Y.; Hu, Y.; Chen, W.; Li, C. Nanostructured Ternary Nanocomposite of rGO/CNTs/MnO₂ for High-Rate Supercapacitors. *ACS Sustainable Chem. Eng.* **2014**, *2*, 70–74.
- (11) Pal, J.; Ganguly, M.; Dutta, S.; Mondal, C.; Negishi, Y.; Pal, T. Hierarchical Au–CuO Nanocomposite from Redox Transformation Reaction for Surface Enhanced Raman Scattering and Clock Reaction. *CrystEngComm* **2014**, *16*, 883–893.
- (12) Wang, Z.; Luan, D.; Li, C. M.; Su, F.; Madhavi, S.; Boey, F. Y. C.; Lou, X. W. Engineering Nonspherical Hollow Structures with Complex Interiors by Template-Engaged Redox Etching. *J. Am. Chem. Soc.* **2010**, *132*, 16271–16277.
- (13) Zhao, Z.; Liu, J.; Cui, F.; Feng, H.; Zhang, L. One-Pot Synthesis of Tunable Fe₃O₄–MnO₂ Core–Shell Nanoplates and Their Applications for Water Purification. *J. Mater. Chem.* **2012**, *22*, 9052–9057.
- (14) Choi, Y.; Hong, S.; Liu, L.; Kim, S. K.; Park, S. Galvanically Replaced Hollow Au–Ag Nanospheres: Study of Their Surface Plasmon Resonance. *Langmuir* **2012**, *28*, 6670–6676.
- (15) Reitz, J. B.; Solomon, E. I. Propylene Oxidation on Copper Oxide Surfaces: Electronic and Geometric Contributions to Reactivity and Selectivity. *J. Am. Chem. Soc.* **1998**, *120*, 11467–11478.
- (16) Poizot, P.; Laruelle, S.; Grugeon, S.; Dupont, L.; Taracón, J.-M. Nano-Sized Transition-Metal Oxides as Negative-Electrode Materials for Lithium–Ion Batteries. *Nature* **2000**, *407*, 496–499.
- (17) Schon, J. H.; Dorget, M.; Beuran, F. C.; Zu, X. Z.; Arushanov, E.; Cavellin, C. D.; Lagues, M. Superconductivity in CaCuO₂ as a Result of Field-Effect Doping. *Nature* **2001**, *414*, 434–436.
- (18) Xu, Y.; Chen, D.; Jiao, X. Fabrication of CuO Prickly Microspheres with Tunable Size by a Simple Solution Route. *J. Phys. Chem. B* **2005**, *109*, 13561–13566.
- (19) Zheng, S.-F.; Hu, J.-S.; Zhong, L.-S.; Song, W.-G.; Wan, L.-J.; Guo, Y.-G. Introducing Dual Functional CNT Networks into CuO Nanomicrospheres toward Superior Electrode Materials for Lithium-Ion Batteries. *Chem. Mater.* **2008**, *20*, 3617–3622.
- (20) Post, J. E. Manganese Oxide Minerals: Crystal Structures and Economic and Environmental Significance. *Proc. Natl. Acad. Sci. U.S.A.* **1999**, *96*, 3447–3454.
- (21) Subramanian, V.; Zhu, H.; Vajtai, R.; Ajayan, P. M.; Wei, B. Hydrothermal Synthesis and Pseudocapacitance Properties of MnO₂ Nanostructures. *J. Phys. Chem. B* **2005**, *109*, 20207–20214.
- (22) Kim, E.-J.; Lee, C.-S.; Chang, Y.-Y.; Chang, Y.-S. Hierarchically Structured Manganese Oxide-Coated Magnetic Nanocomposites for the Efficient Removal of Heavy Metal Ions from Aqueous Systems. *ACS Appl. Mater. Interfaces* **2013**, *5*, 9628–9634.
- (23) Sinha, A. K.; Pradhan, M.; Pal, T. Morphological Evolution of Two-Dimensional MnO₂ Nanosheets and Their Shape Transformation to One-Dimensional Ultralong MnO₂ Nanowires for Robust Catalytic Activity. *J. Phys. Chem. C* **2013**, *117*, 23976–23986.
- (24) Miyazaki, K.; Hieda, M.; Kato, T. Development of a Novel Manganese Oxide–Clay Humidity Sensor. *Ind. Eng. Chem. Res.* **1997**, *36*, 88–91.
- (25) Qian, K.; Qian, Z.; Hua, Q.; Jiang, Z.; Huang, W. Structure–Activity Relationship of CuO/MnO₂ Catalysts in CO Oxidation. *Appl. Surf. Sci.* **2013**, *273*, 357–363.
- (26) Angeles-Hernandez, M. J.; Leeke, G. A.; Santos, R. C. D. Catalytic Supercritical Water Oxidation for the Destruction of Quinoline over MnO₂/CuO Mixed Catalyst. *Ind. Eng. Chem. Res.* **2009**, *48*, 1208–1214.
- (27) Martin, A.; Armbruster, U.; Schneider, M.; Radnik, J.; Pohl, M.-M. Structural Transformation of an Alumina-Supported MnO₂–CuO Oxidation Catalyst by Hydrothermal Impact of Sub- and Supercritical Water. *J. Mater. Chem.* **2002**, *12*, 639–645.
- (28) Tafesh, A. M.; Weiguny, J. A Review of the Selective Catalytic Reduction of Aromatic Nitro Compounds into Aromatic Amines, Isocyanates, Carbamates, and Ureas Using CO. *Chem. Rev.* **1996**, *96*, 2035–2052.
- (29) Shi, Q.; Lu, R.; Lu, L.; Fu, X.; Zhao, D. Efficient Reduction of Nitroarenes over Nickel-Iron Mixed Oxide Catalyst Prepared from a Nickel-Iron Hydroxalite Precursor. *Adv. Synth. Catal.* **2007**, *349*, 1877–1881.
- (30) Wunder, S.; Polzer, F.; Lu, Y.; Mei, Y.; Ballauff, M. Kinetic Analysis of Catalytic Reduction of 4-Nitrophenol by Metallic Nanoparticles Immobilized in Spherical Polyelectrolyte Brushes. *J. Phys. Chem. C* **2010**, *114*, 8814–8820.
- (31) Layek, K.; Kantam, M. L.; Shirai, M.; Nishio-Hamane, D.; Sasakid, T.; Maheswarana, H. Gold Nanoparticles Stabilized on Nanocrystalline Magnesium Oxide as an Active Catalyst for Reduction of Nitroarenes in Aqueous Medium at Room Temperature. *Green Chem.* **2012**, *14*, 3164–3174.
- (32) Pradhan, N.; Pal, A.; Pal, T. Catalytic Reduction of Aromatic Nitro Compounds by Coinage Metal Nanoparticles. *Langmuir* **2001**, *17*, 1800–1802.
- (33) Sarkar, S.; Sinha, A. K.; Pradhan, M.; Basu, M.; Negishi, Y.; Pal, T. Redox Transmetalation of Prickly Nickel Nanowires for Morphology Controlled Hierarchical Synthesis of Nickel/Gold Nanostructures for Enhanced Catalytic Activity and SERS Responsive Functional Material. *J. Phys. Chem. C* **2011**, *115*, 1659–1673.
- (34) Khalavka, Y.; Becker, J.; Sönnichsen, C. Synthesis of Rod-Shaped Gold Nanorattles with Improved Plasmon Sensitivity and Catalytic Activity. *J. Am. Chem. Soc.* **2009**, *131*, 1871–1875.
- (35) Johnson, J. A.; Makis, J. J.; Marvin, K. A.; Rodenbusch, S. E.; Stevenson, K. J. Size-Dependent Hydrogenation of p-Nitrophenol with

Pd Nanoparticles Synthesized with Poly(amido)amine Dendrimer Templates. *J. Phys. Chem. C* **2013**, *117*, 22644–22651.

(36) Kalekar, A. M.; Sharma, K. K. K.; Lehoux, A.; Audonnet, F.; Remita, H.; Saha, A.; Sharma, G. K. Investigation into the Catalytic Activity of Porous Platinum Nanostructures. *Langmuir* **2013**, *29*, 11431–11439.

(37) Antonels, N. C.; Meijboom, R. Preparation of Well-Defined Dendrimer Encapsulated Ruthenium Nanoparticles and Their Evaluation in the Reduction of 4-Nitrophenol According to the Langmuir–Hinshelwood Approach. *Langmuir* **2013**, *29*, 13433–13442.

(38) Pal, J.; Ganguly, M.; Mondal, C.; Roy, A.; Negishi, Y.; Pal, T. Crystal-Plane-Dependent Etching of Cuprous Oxide Nanoparticles of Varied Shapes and Their Application in Visible Light Photocatalysis. *J. Phys. Chem. C* **2013**, *117*, 24640–24653.

(39) Tang, B.; Wang, G.; Zhuo, L. H.; Ge, J. Novel Dandelion-Like Beta-Manganese Dioxide Microstructures and Their Magnetic Properties. *Nanotechnology* **2006**, *17*, 947–951.

(40) Zhang, Y.; Deng, B.; Zhang, T.; Gao, D.; Xu, A.-W. Shape Effects of Cu₂O Polyhedral Microcrystals on Photocatalytic Activity. *J. Phys. Chem. C* **2010**, *114*, 5073–5079.

(41) Ho, J.-Y.; Huang, M. H. Synthesis of Submicrometer-Sized Cu₂O Crystals with Morphological Evolution from Cubic to Hexapod Structures and Their Comparative Photocatalytic Activity. *J. Phys. Chem. C* **2009**, *113*, 14159–14164.

(42) Hua, Q.; Cao, T.; Bao, H.; Jiang, Z.; Huang, W. Crystal-Plane-Controlled Surface Chemistry and Catalytic Performance of Surfactant-Free Cu₂O Nanocrystals. *ChemSusChem* **2013**, *6*, 1966–1972.

(43) Li, L.; Nan, C.; Peng, Q.; Li, Y. Selective Synthesis of Cu₂O Nanocrystals as Shape-Dependent Catalysts for Oxidative Arylation of Phenylacetylene. *Chem.—Eur. J.* **2012**, *18*, 10491–10496.

(44) Chanda, K.; Rej, S.; Huang, M. H. Facet-Dependent Catalytic Activity of Cu₂O Nanocrystals in the One-Pot Synthesis of 1,2,3-Triazoles by Multicomponent Click Reactions. *Chem.—Eur. J.* **2013**, *19*, 16036–16043.

(45) Bao, H.; Zhang, W.; Shang, D.; Hua, Q.; Ma, Y.; Jiang, Z.; Yang, J.; Huang, W. Shape-Dependent Reducibility of Cuprous Oxide Nanocrystals. *J. Phys. Chem. C* **2010**, *114*, 6676–6680.

(46) Hua, Q.; Shang, D.; Zhang, W.; Chen, K.; Chang, S.; Ma, Y.; Jiang, Z.; Yang, J.; Huang, W. Morphological Evolution of Cu₂O Nanocrystals in an Acid Solution: Stability of Different Crystal Planes. *Langmuir* **2011**, *27*, 665–671.

(47) Hua, Q.; Chen, K.; Chang, S.; Ma, Y.; Huang, W. Crystal Plane-Dependent Compositional and Structural Evolution of Uniform Cu₂O Nanocrystals in Aqueous Ammonia Solutions. *J. Phys. Chem. C* **2011**, *115*, 20618–20627.

(48) Huang, W.-C.; Lyu, L.-M.; Yang, Y.-C.; Huang, M. H. Synthesis of Cu₂O Nanocrystals from Cubic to Rhombic Dodecahedral Structures and Their Comparative Photocatalytic Activity. *J. Am. Chem. Soc.* **2012**, *134*, 1261–1267.

(49) Bao, H.; Zhang, W.; Hua, Q.; Jiang, Z.; Yang, J.; Huang, W. Crystal-Plane-Controlled Surface Restructuring and Catalytic Performance of Oxide Nanocrystals. *Angew. Chem., Int. Ed.* **2011**, *50*, 12294–12298.

(50) Vaidya, M. J.; Kulkarni, S. M.; Chaudhari, R. V. Synthesis of p-Aminophenol by Catalytic Hydrogenation of p-Nitrophenol. *Org. Process Res. Dev.* **2003**, *7*, 202–208.

(51) Xu, Y.; Wang, H.; Yu, Y.; Tian, L.; Zhao, W.; Zhang, B. Cu₂O Nanocrystals: Surfactant-Free Room-Temperature Morphology-Modulated Synthesis and Shape-Dependent Heterogeneous Organic Catalytic Activities. *J. Phys. Chem. C* **2011**, *115*, 15288–15296.

(52) Vaseem, M.; Umar, A.; Hahn, Y. B.; Kim, D. H.; Lee, K. S.; Jang, J. S.; Lee, J. S. Flower-Shaped CuO Nanostructures: Structural, Photocatalytic, and XANES Studies. *Catal. Commun.* **2008**, *10*, 11–16.

(53) Liu, L.; Gu, X.; Cao, Y.; Yao, X.; Zhang, L.; Tang, C.; Gao, F.; Dong, L. Crystal-Plane Effects on the Catalytic Properties of Au/TiO₂. *ACS Catal.* **2013**, *3*, 2768–2775.

(54) Cui, E.; Lu, G. New Evidence for the Regulation of Photogenerated Electron Transfer on Surface Potential Energy Controlled Co-catalyst on TiO₂—The Investigation of Hydrogen Production over Selectively Exposed Au Facet on Au/TiO₂. *Int. J. Hydrogen Energy* **2014**, *39*, 7672–7685.

(55) Keil, P.; Lutzenkirchen-Hecht, D.; Frahm, R. Investigation of Room Temperature Oxidation of Cu in Air by Yoneda- XAFS. *AIP Conf. Proc.* **2007**, *882*, 490–492.